

---

# DEEP REINFORCEMENT LEARNING ACHIEVES FLOW CONTROL OF THE 2D KÁRMÁN VORTEX STREET

---

**Jean Rabault**

Department of Mathematics  
University of Oslo  
jean.rblt@gmail.com

**Ulysse Reglade**

CEMEF, Mines ParisTech  
ulysse.reglade@mines-paristech.fr

**Nicolas Cerardi**

CEMEF, Mines ParisTech  
nicolas.cerardi@mines-paristech.fr

**Miroslav Kuchta**

Department of Mathematics  
University of Oslo  
mirok@math.uio.no

**Atle Jensen**

Department of Mathematics  
University of Oslo  
atlej@math.uio.no

September 3, 2018

## ABSTRACT

The Kármán Vortex Street has been investigated for over a century and offers a reference case for investigation of flow stability and control of high dimensionality, non-linear systems. Active flow control, while of considerable interest from a theoretical point of view and for industrial applications, has remained inaccessible due to the difficulty in finding successful control strategies. Here we show that Deep Reinforcement Learning can achieve a stable active control of the Kármán vortex street behind a two-dimensional cylinder. Our results show that Deep Reinforcement Learning can be used to design active flow controls and is a promising tool to study high dimensionality, non-linear, time dependent dynamic systems present in a wide range of scientific problems.

**Keywords** Active Flow Control · Artificial Neural Network · Deep Reinforcement Learning

## 1 Introduction

The flow past a circular cylinder is a famous, intensively studied problem in fluid mechanics. Above a critical Reynolds number (which measures the relative importance of inertia and viscosity in a flow and is written as  $Re = UL/\nu$ , where  $U$  is the typical velocity in the flow,  $L$  a typical length scale, and  $\nu$  the kinematic viscosity), the flow results in an organized vortex street that has been studied since the beginning of the 20th century Von Kármán (1911). While the transition to unsteady flow at a critical Reynolds number  $Re_{cr} \approx 46$  has been identified as a supercritical Hopf bifurcation Provansal *et al.* (1987), a number of complex phenomena, some of which are still under discussion, make the situation complex as  $Re$  is increased. The detailed mechanisms behind the instability of the time-dependent vortex street have been the subject of controversies in the past Kida (1982); Saffman & Schatzman (1982) and are still an active field of research Mowlavi *et al.* (2016); Heil *et al.* (2017), while attempts to perform active flow control face considerable challenges. Flow control is made challenging due to the unsteady, non-linear, high dimensionality behavior implied by the Navier-Stokes (NS) equations as soon as inertia becomes important Marquet *et al.* (2008); Barbagallo *et al.* (2012). Among the approaches used to attack this problem, the methods based on the adjoint formulation of the optimal control, e.g. Li *et al.* (2003), require a potentially large number of solutions to the adjoint system (in particular if the problem at hand is ill-posed), and are thus hard to scale. A different class of approaches is based on building a lower-dimensional representation of the flow, e.g. by projecting the full model onto a lower dimensional state space obtained for example by Proper Orthogonal Decomposition or Dynamic Mode Decomposition Ravindran (2000). However, the dimensionality of the space typically grows with  $Re$  making construction of the models expensive. Furthermore, the models may not be robust to changes of  $Re$  outside of the training/construction range Brunton & Noack (2015). While strategies based on such models obtain good results on specific applications Atam *et al.* (2017),

these methods are difficult to apply to strongly nonlinear dynamic systems and are very specific of a given configuration Brunton & Noack (2015). As a consequence, a recent review of the field of active flow control calls to embrace the Artificial Intelligence (AI) and Machine Learning paradigm to perform control of complex high-dimensional systems Brunton & Noack (2015). This view is confirmed by recent experiments of closed-loop control Debien *et al.* (2016), Gautier *et al.* (2015), Benard *et al.* (2016) where AI techniques, in particular genetic programming, were applied with success.

Artificial intelligence and the machine learning paradigm are made even more attractive by several recent highly profiled successes of Deep Artificial Neural Networks (DANNs), such as attaining super-human performance at image labeling LeCun *et al.* (2015), crushing the leading human player at the game of Go Silver *et al.* (2017), or achieving control of complex robots Gu *et al.* (2017), which have shed the light on their ability to handle complex, non-linear systems. In particular, the Deep Reinforcement Learning (DRL) methodology is a promising avenue for the control of complex systems. This approach consists in letting the DANN interact with the system it should control through 3 channels: an observation of the state of the system, a control imposed by the network on the system, and a reward function measuring control performance. The choice of the reward function allows to direct the efforts of the DANN towards solving a specific problem.

Here, we present the first successful use of DANNs trained through DRL to attack the problem of active flow control in a 2D simulation of the flow around a cylinder at a moderate value of the Reynolds number,  $Re = 100$  ( $Re$  is computed based on the cylinder diameter, for more details see the Supplementary Information). This is an illustration of the potential of Artificial Neural Networks trained through Deep Reinforcement Learning for studying and controlling high dimensionality, non-linear systems.

## 2 Active flow control in a simulation

To demonstrate the ability of DANNs trained through DRL to perform active flow control, we set up a simple 2D simulation of the non-dimensionalized flow around a cylinder as described by the incompressible NS equations at  $Re = 100$ . The configuration chosen is a copy of a classical benchmark used for the validation of numerical codes Schäfer *et al.* (1996). In addition, two small jets of angular width  $10^\circ$  are set on the sides of the cylinder and inject fluid in the direction normal to the cylinder surface, following the control set up by the DANN. This implies that the control relies on influencing the separation of the Kármán vortices, rather than direct injection of momentum as could be obtained through propulsion. The jets are controlled through their mass flow rates, respectively  $Q_1$  and  $Q_2$ . We choose to use synthetic jets, meaning that no net mass flow rate is injected in the flow, which translates to the constraint  $Q_1 + Q_2 = 0$ . More details are available in the Supplementary Information.

The aim of the control strategy is guided by the reward function fed to the DRL during training. In the present work, we want to minimize the drag  $D$  through a reduction in the strength of the vortex shedding. For this, we define the reward function  $r$  from both the drag  $D$  and the lift  $L$ , following:

$$r = \langle D \rangle_T - |\langle L \rangle_T|,$$

where  $\langle \bullet \rangle_T$  indicates the mean over one full vortex shedding cycle. In the figures, we present the value of the drag coefficient, which is a normalized value of the drag  $C_D = \frac{D}{\rho \bar{U}^2 R}$ , where  $\bar{U} = 2U(0)/3$  is the mean velocity magnitude,  $\rho$  the volumetric mass density of the fluid, and  $R$  the diameter of the cylinder (for more details, see the Supplementary Information). Similarly, the mass flow rates of the jets are normalized as  $Q_i^* = Q_i/Q_c$ , where  $Q_c = \int_{-R}^R \rho U(y) dy$  is the mass flow rate introduced by the inlet profile that intersects the cylinder diameter. Therefore,  $Q_i^*$  indicates the relative strength of the control jets, compared with the incoming flow.

Drastic changes are observed in the flow behind the cylinder in the case of active flow control by a trained DANN compared with the baseline simulation without control, as visible in Fig. 1. A video of the flow undergoing active control, compared with the baseline, is also available as Extended Data. The vortex shedding is both strongly reduced in intensity, and displaced around 3 cylinder diameters downstream of the cylinder. The change in the flow configuration has a notable effect on both the lift and drag: drag is reduced by around 8% (see Fig. 2), while the fluctuations in lift are reduced by around 75%. The area  $A$  of the recirculation bubble is drastically increased, by 125%. In addition, the vortex shedding frequency is modified by the active control, and gets reduced by around 15%.

The explanation for the reduced drag is to be found in the change of the mean pressure distribution around the cylinder. As visible in Fig. 3, the recirculation area behind the cylinder undergoing active control is both larger, and less intense than in the baseline case. This somewhat counter-intuitive effect is a good illustration of the ability of the DANN to find complex strategies to optimize its reward function.

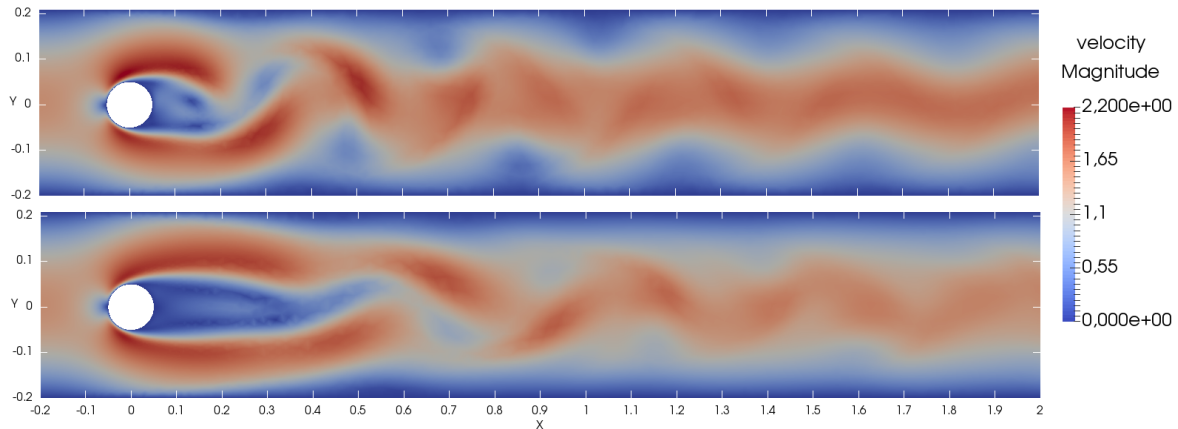


Figure 1: Snapshots of the velocity magnitude illustrating the effect of the active flow control. Top: baseline simulation. Bottom: result with active flow control. The size of the recirculation bubble is greatly increased in the case with active control, and the strength of the Kármán vortex street is reduced. A video comparing the two flows is available as Extended Data.

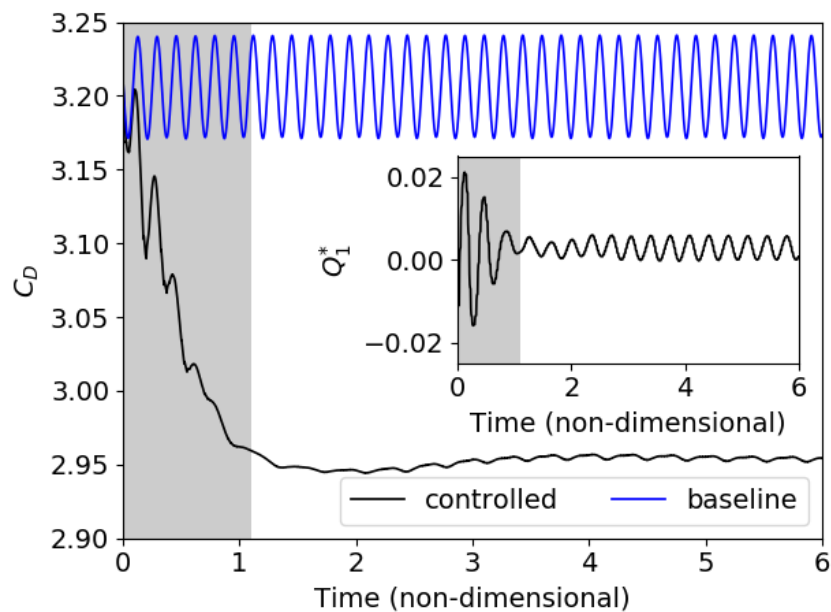


Figure 2: Time-resolved value of the drag coefficient  $C_D$  in the case without (baseline curve) and with (controlled curve) active flow control, and corresponding normalized mass flow rate of the control jet 1 (inset). The effect of the flow control on the drag is clearly visible: a reduction of the drag of around 8% is observed, and the fluctuations in time due to vortex shedding are nearly suppressed. Two phases can be distinguished in the mass flow rate control: first, a relatively large control is used to change the flow configuration, up to a non-dimensional time of around 1.1, before a pseudo periodic regime with very limited flow control is established.

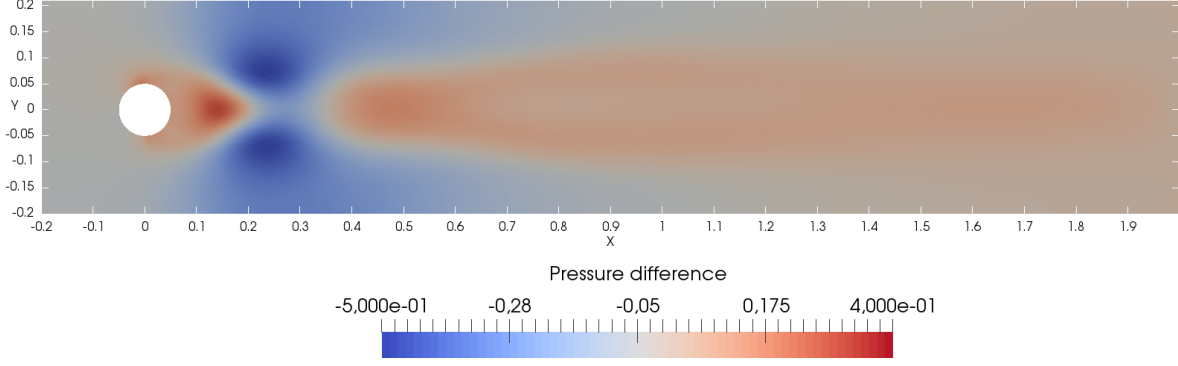


Figure 3: Difference between the mean pressure field in the actuation case and the baseline case. The pressure in the recirculation bubble is increased by the actuation, which is the cause for the drag reduction.

Finally, it should be noted that very little mass flow rate is necessary to perform active flow control, as visible in Fig. 2. Two phases are visible on Fig. 2, and also on the video in the Extended Data. First, a very short transient takes place where the DANN changes the flow configuration. Then, the DANN manages to keep the flow in this modified configuration, performing a pseudo-periodic control. While we give the DANN the freedom to set a control mass flow rate for each jet in the range of  $Q_i^* = [-0.07, +0.07]$ , in practice the network chooses to use normalized mass flow rates of absolute value at most 0.02 during the initial transient control, and as small as  $5 \times 10^{-3}$  at most to keep the vortex street in its new regime. This represents in average only around 0.35% of the incoming mass flow rate that intercepts the diameter of the cylinder for the active flow control in the established regime. Despite the very limited level of actuation in the new pseudo-periodic flow regime, altering the control signal even slightly leads to a collapse of the active control.

### 3 Discussion and future work

We prove that DANNs trained through DRL are a possible tool for performing active flow control. It is striking to see how efficient the DANN can be, as we show that our trained network uses very small controls to play with the state of a complex system. From the shape of the control signal, it seems that the DANN finds ways to control the flow through infinitesimal modifications of exponentially amplified modes that control the detachment of the vortex street, a fact that was previously reported in attempts to perform optimal flow control on simplified reduced order models Atam *et al.* (2017).

Following our results, it appears that DANNs trained through DRL could have a general interest in fluid mechanics. Indeed, we have proved their relevance for active flow control, and a number of interesting cases should be investigated, such as the control of 3D Large Eddy Simulations, or Direct Numerical Simulation of boundary layers. In addition, one could try to combine DANNs with more traditional analytical methods to investigate properties of the solutions implied by the NS equations. Moreover, besides fluid mechanics, our work suggests that the use of DANNs as an experimental tool to study complex systems where traditional analytical approaches are limited should be investigated. In this sense, our results can be seen as one more confirmation of the main message expressed in the last years by the community investigating DANNs: DANNs are a successful tool at studying and handling complexity, which under its many forms is one of the major challenges modern science still fails to fully apprehend.

### 4 Acknowledgments

We gratefully acknowledge funding by the Research Council of Norway through the grants 'DOFI' (grant number 280625) and 'RigSpray' (grant number 421160). We are grateful to Terje Kvernes and Lucy Karpen for considerable help setting up the computation infrastructure used in this project.

### References

ABADI, MARTÍN, BARHAM, PAUL, CHEN, JIANMIN, CHEN, ZHIFENG, DAVIS, ANDY, DEAN, JEFFREY, DEVIN, MATTHIEU, GHEMAYAT, SANJAY, IRVING, GEOFFREY, ISARD, MICHAEL & OTHERS 2016 Tensorflow: A system for large-scale machine learning. In *OSDI*, , vol. 16, pp. 265–283.

- ATAM, E., MATHELIN, L. & CORDIER, L. 2017 Identification-based closed-loop control strategies for a cylinder wake flow. *IEEE Transactions on Control Systems Technology* **25** (4), 1488–1495.
- BARBAGALLO, ALEXANDRE, DERGHAM, GREGORY, SIPP, DENIS, SCHMID, PETER J. & ROBINET, JEAN-CHRISTOPHE 2012 Closed-loop control of unsteadiness over a rounded backward-facing step. *Journal of Fluid Mechanics* **703**, 326–362.
- BENARD, N, PONS-PRATS, JORDI, PERIAUX, J, BUGEDA, G, BRAUD, P, BONNET, JP & MOREAU, E 2016 Turbulent separated shear flow control by surface plasma actuator: Experimental optimization by genetic algorithm approach. *Experiments in Fluids* **57** (2), 22.
- BRUNTON, STEVEN L & NOACK, BERND R 2015 Closed-loop turbulence control: progress and challenges. *Applied Mechanics Reviews* **67** (5), 050801.
- DEBIEN, ANTOINE, VON KRBEK, KAI AFF, MAZELLIER, NICOLAS, DURIEZ, THOMAS, CORDIER, LAURENT, NOACK, BERND R, ABEL, MARKUS W & KOURTA, AZEDDINE 2016 Closed-loop separation control over a sharp edge ramp using genetic programming. *Experiments in fluids* **57** (3), 40.
- GAUTIER, NICOLAS, AIDER, J-L, DURIEZ, THOMAS, NOACK, BR, SEGOND, MARC & ABEL, MARKUS 2015 Closed-loop separation control using machine learning. *Journal of Fluid Mechanics* **770**, 442–457.
- GEUZAIN, CHRISTOPHE & REMACLE, JEAN-FRANÇOIS 2009 Gmsh: A 3-D finite element mesh generator with built-in pre-and post-processing facilities. *International journal for numerical methods in engineering* **79** (11), 1309–1331.
- GODA, KATUHIKO 1979 A multistep technique with implicit difference schemes for calculating two- or three-dimensional cavity flows. *Journal of Computational Physics* **30** (1), 76 – 95.
- GU, S., HOLLY, E., LILICRAP, T. & LEVINE, S. 2017 Deep reinforcement learning for robotic manipulation with asynchronous off-policy updates. In *2017 IEEE International Conference on Robotics and Automation (ICRA)*, pp. 3389–3396.
- HEIL, MATTHIAS, ROSSO, JORDAN, HAZEL, ANDREW L & BRØNS, MORTEN 2017 Topological fluid mechanics of the formation of the Kármán-vortex street. *Journal of Fluid Mechanics* **812**, 199–221.
- KIDA, SHIGEO 1982 Stabilizing effects of finite core on Kármán vortex street. *Journal of Fluid Mechanics* **122**, 487–504.
- LECUN, YANN, BENGIO, YOSHUA & HINTON, GEOFFREY 2015 Deep learning. *Nature* **521** (7553), 436.
- LI, ZHIJIN, NAVON, IM, HUSSAINI, MY & LE DIMET, F-X 2003 Optimal control of cylinder wakes via suction and blowing. *Computers & Fluids* **32** (2), 149–171.
- LOGG, ANDERS, MARDAL, KENT-ANDRE & WELLS, GARTH 2012 *Automated solution of differential equations by the finite element method: The FEniCS book*, , vol. 84. Springer Science & Business Media.
- MARQUET, OLIVIER, SIPP, DENIS & JACQUIN, LAURENT 2008 Sensitivity analysis and passive control of cylinder flow. *Journal of Fluid Mechanics* **615**, 221–252.
- MOWLAVI, SAVIZ, ARRATIA, CRISTÓBAL & GALLAIRE, FRANÇOIS 2016 Spatio-temporal stability of the Kármán vortex street and the effect of confinement. *Journal of Fluid Mechanics* **795**, 187–209.
- PROVANSAL, M, MATHIS, C & BOYER, L 1987 Bénard-von Kármán instability: transient and forced regimes. *Journal of Fluid Mechanics* **182**, 1–22.
- RAVINDRAN, SIVAGURU S 2000 A reduced-order approach for optimal control of fluids using proper orthogonal decomposition. *International journal for numerical methods in fluids* **34** (5), 425–448.
- SAFFMAN, PG & SCHATZMAN, JC 1982 An inviscid model for the vortex-street wake. *Journal of Fluid Mechanics* **122**, 467–486.
- SCHAARSCHMIDT, MICHAEL, KUHNLE, ALEXANDER & FRICKE, KAI 2017 Tensorforce: A Tensorflow library for applied reinforcement learning. Web page.

- SCHÄFER, M., TUREK, S., DURST, F., KRAUSE, E. & RANNACHER, R. 1996 *Benchmark Computations of Laminar Flow Around a Cylinder*, pp. 547–566. Wiesbaden: Vieweg+Teubner Verlag.
- SCHULMAN, JOHN, WOLSKI, FILIP, DHARIWAL, PRAFULLA, RADFORD, ALEC & KLIMOV, OLEG 2017 Proximal policy optimization algorithms. *arXiv preprint arXiv:1707.06347* .
- SILVER, DAVID, SCHRITTWIESER, JULIAN, SIMONYAN, KAREN, ANTONOGLU, IOANNIS, HUANG, AJA, GUEZ, ARTHUR, HUBERT, THOMAS, BAKER, LUCAS, LAI, MATTHEW, BOLTON, ADRIAN & OTHERS 2017 Mastering the game of Go without human knowledge. *Nature* **550** (7676), 354.
- VALEN-SENDSTAD, KRISTIAN, LOGG, ANDERS, MARDAL, KENT-ANDRE, NARAYANAN, HARISH & MORTENSEN, MIKAEL 2012 A comparison of finite element schemes for the incompressible Navier–Stokes equations. In *Automated Solution of Differential Equations by the Finite Element Method*, pp. 399–420. Springer.
- VON KÁRMÁN, TH 1911 Über den mechanismus des widerstandes, den ein bewegter körper in einer flüssigkeit erfährt. *Nachrichten von der Gesellschaft der Wissenschaften zu Göttingen, Mathematisch-Physikalische Klasse* **1911**, 509–517.

## 5 Supplementary Information

Here we present some additional details regarding the simulation set-up, the DANN, and the DRL algorithm used. All the code used for both the simulation and the DANN trained through DRL is based on open source packages (respectively, FEniCS Logg *et al.* (2012), Tensorforce Abadi *et al.* (2016) and Tensorflow, Schaarschmidt *et al.* (2017)). All code is made available on the Github repository of the corresponding author [will be released upon publication].

### 5.1 Simulation

The 2D simulation environment is non-dimensionalized. Following the baseline Schäfer *et al.* (1996), it consists of a cylinder of radius  $R = 0.05$  immersed in a box of total length  $L = 2.2$  along the X-axis and height  $H = 0.41$  along the Y-axis. The kinematic viscosity is set as  $\nu = 10^{-3}$ , the fluid volumetric mass density is  $\rho = 1$ . The origin of the coordinate system is at the center of the cylinder. The inflow profile (set on the left wall) is parabolic, and follows the formula (cf. 2D-2 test case in Schäfer *et al.* (1996)):

$$U(y) = 4U_m(H/2 - y)(H/2 + y)/H^2,$$

where  $(U(y), V(y) = 0)$  is the velocity vector. We follow the baseline in choosing  $U_m = 1.5$ . A no slip boundary condition is imposed on the top and bottom walls and on the solid walls of the cylinder. The outflow boundary condition is imposed on the right wall of the domain. The Reynolds number, based on the mean velocity magnitude  $\bar{U} = 2U(0)/3$ , is  $Re = 2R\bar{U}/\nu = 100$ . The domain is discretized using Gmsh Geuzaine & Remacle (2009). With the mesh refined in the vicinity of the cylinder the computational domain consists of a total number of 7142 triangular elements. A non-dimensional, constant numerical time step  $dt = 5 \cdot 10^{-4}$  is used. Moreover, two additional refined meshes, counting up to 30000 elements, were used for performing a mesh refinement study. The difference in drag between the coarsest and the finest mesh is under 1%, therefore the coarsest mesh appears suitable for performing our computations. In the case of the finest mesh, the time step had to be reduced to  $dt = 3 \cdot 10^{-4}$  to avoid violating the CFL conditions and preventing the simulation from diverging.

In the interest of short solution time, the governing Navier-Stokes equations are solved in a segregated manner Valen-Sendstad *et al.* (2012). More precisely, the Incremental Pressure Correction Scheme (IPCS method, Goda (1979)) with an explicit treatment of the nonlinear term is used. Spatial discretization then relies on the finite element method implemented within the FEniCS framework Logg *et al.* (2012).

As stated in the main text, the jets are normal to the cylinder wall and are implemented on the sides of the cylinder, at angles  $\theta_1 = 90^\circ$  and  $\theta_2 = 270^\circ$  relative to the flow direction. The jets are controlled through their mass flow rate,  $Q_i$ ,  $i = 1, 2$ , and are set through a parabolic velocity profile going to zero at the edges of the jet. The jet width is set to  $10^\circ$ .

Finally, information is extracted from the simulation and provided to the DRL agent. 151 pressure probes are located in the vicinity of the cylinder and in its wake. The total drag  $D$  on the cylinder  $C$  is computed following:

$$D = \int_C (\sigma \cdot n) \cdot e_x dS,$$

where  $\sigma$  is the Cauchy stress tensor,  $n$  is the outer unit normal vector of the cylinder surface and  $e_x = (1, 0)$ .

A benchmark of the simulation was performed by observing the drag value, the pressure fluctuations and the Strouhal number  $St = fL/\bar{U}$ , where  $f$  is the vortex shedding frequency. Results are in good agreement with previously published data Schäfer *et al.* (1996). For example, we observe a mean absolute value of the non-dimensional drag without actuation of  $D = 0.16$ , which corresponds to a drag coefficient  $C_D = \frac{D}{\rho\bar{U}^2R} \approx 3.2$ , in excellent agreement with the results reported by Schäfer *et al.* (1996) who obtain, depending on the solver used, a mean drag coefficient of typically 3.19 to 3.22.

### 5.2 Artificial Neural Network and Deep Reinforcement Learning algorithm

The DANN is a simple fully connected network, featuring one input layer, two consecutive fully connected hidden layers of size 512 neurons each, and one output layer. The classical rectified linear unit (ReLU) of positive slope 1 is used as an activation function. The input layer is connected to the 151 probes immersed in the simulation that measure the value of the flow velocity in the vicinity of the cylinder. The output layer sets the mass flow rates of the jets. The DRL algorithm used for training, known in the literature as the Proximal Policy Optimization method (PPO Schulman *et al.* (2017)), is the current state-of-the-art for training DANNs to perform continuous control. Each training epoch is started from a converged, well-defined Kármán vortex street. An episode duration lasts around 8 vortex shedding periods.

As stated in the main body of the article, we define the reward function  $r$  from both the drag  $D$  and the lift  $L$ , following:

$$r = \langle D \rangle_T - |\langle L \rangle_T|,$$

where  $\langle \bullet \rangle_T$  indicates the mean over one full vortex shedding cycle.

It is difficult for the PPO algorithm to learn the necessity to set time-correlated, continuous control signals. This is a consequence of the PPO trying at first purely random controls. Therefore, we added two limitations to the control. First, the control value provided by the network is kept constant for a duration of around 10% of the vortex shedding period. Second, the control effectively set in the simulation is made continuous in time. To this end, the control at each time step in the simulation is obtained for each jet as  $c_{s+1} = c_s + \alpha(a - c_s)$ , where  $c_s$  is the control of the jet considered at the previous numerical time step,  $c_{s+1}$  is the new control,  $a$  is the action provided by the PPO agent for the current set of time steps, and  $\alpha = 0.1$  is a numerical parameter. In practice, the exact value of  $\alpha$  has little to say over the performance of the control.

It takes around 120 training epochs, lasting altogether for about one night on a standard desktop computer using 1 CPU core, for the DANN to learn a reasonably converged strategy similar to what is shown in the main body of the text.

## 6 Multimedia files

A video showing the velocity magnitude obtained both in the baseline case with no control (top) and in the case with active control (bottom) on the same color scale is provided here: [https://folk.uio.no/jeanra/Research/comparison\\_baseline\\_actuation.avi](https://folk.uio.no/jeanra/Research/comparison_baseline_actuation.avi). The actuation jets are quite visible in the first frames of the video, corresponding to the initial phase when the DANN modifies the flow configuration. Later on, the jets are so weak that they are barely visible. Nonetheless, the weak actuation is vital to maintain flow control.